


ARTICLE



Targeting lectin-like oxidized low-density lipoprotein receptor-1 triggers autophagic program in esophageal cancer

Can Li^{1,5}, Fenglin Liu^{2,5}, Xu Yang^{1,5}, Bao Guo¹, Guoyun Li³, Jie Yin², Gaofei He¹, Caiting Yang⁴, Ling Xu¹, Shuxuan Li¹, Hao Wu¹, Hai Liu⁴, Yuanyuan Ruan¹, Jianxin Gu¹ and Lan Wang¹ 

© The Author(s), under exclusive licence to ADMC Associazione Differenziamento e Morte Cellulare 2021

Autophagy is a highly conserved catabolic process to maintain cellular homeostasis. However, dysfunctional autophagy contributes to a context-dependent role in cancer. Here, we clarified the exact role of autophagy modulated by the scavenger receptor lectin-like oxidized low-density lipoprotein receptor-1 (LOX-1) in esophageal cancer (EC). A comprehensive analysis in various cancers displayed that LOX-1 was upregulated the most in EC tissues and associated with poor prognosis of patients. Deletion of LOX-1 *ex vivo* and *in vivo* suppresses EC development by inducing autophagic cell death. Receptor for activated C kinase 1 (RACK1) was identified as a signal adapter of LOX-1, which incited RAS/MEK/ERK pathway and TFEB nuclear export signal and safeguarded tumorigenesis. A sulfated polysaccharide fucoidan extracted from brown seaweed was found to bind with LOX-1 and mediate its proteasomal degradation but not the lysosome pathway, leading to autophagy-related cell death in EC. These results reveal a central contribution of LOX-1 to EC development and provide genetic ablation or bioactive polysaccharide as an effective intervention for EC therapy.

Cell Death & Differentiation (2022) 29:697–708; <https://doi.org/10.1038/s41418-021-00884-y>

INTRODUCTION

Esophageal cancer (EC) is a lethal malignancy with strong regional distribution [1]. The more common type of EC globally is still esophageal squamous cell carcinoma (ESCC), of which 79% of cases occurred in Asia [2]. The exact etiology of ESCC remains unclear. Most studies believe that the occurrence of esophageal mucosal epithelial tumors is due to a combination of multiple factors and long-term chronic stimulation. Although the 5-year survival rate of patients with EC has been improved with the advancement of diagnosis and treatment technology, it is still at a low level of 10–30% worldwide [3]. Thus, a better understanding of the molecular mechanism is necessary to achieve precise prevention and treatment of EC.

Autophagy is an intracellular self-digesting system that delivers protein aggregates or damaged organelles to lysosomes [4]. In cancer, the role of autophagy remains controversial, which depends on the type, stage, and genetic background of cancer [5]. Autophagy helps cancer cells survive in adverse conditions like chemotherapy [6] and radiotherapy [7], while prolonged or excessive activation of autophagy induces autophagy-related cell death in cancer cells [8, 9]. Hence, although the current clinical focus is to combine autophagy inhibitors with chemotherapeutic drugs, the contradictory role of autophagy in inhibiting tumor growth at the initial stage and whether excessive autophagy can lead to cell death should still be considered.

Lectin-like oxidized low-density lipoprotein receptor-1 (LOX-1, also known as *OLR1*) belongs to the C-type lectin superfamily on chromosome 12 [10]. Compared with other C-type lectin members, the Dectin-1 gene clusters, including *MICL*, *CLECT1A*, *CLECT1B*, *CLECT12B*, *CLECT9A*, *Dectin-1*, and *OLR1*, possess a wider range of functions and ligands [11]. As a major scavenger receptor, LOX-1 can recognize and internalize ox-LDL, and current researches focused on LOX-1 of vascular-related cells and its biological function in atherosclerosis [12]. In vascular smooth muscle cells, a modest amount of ox-LDL has been reported to increase reactive oxygen species (ROS) formation and strongly contribute to oxidative DNA damage leading to autophagy [13]. While in this study, we reveal a comprehensive and novel perspective of the autophagic program controlled by LOX-1 in EC.

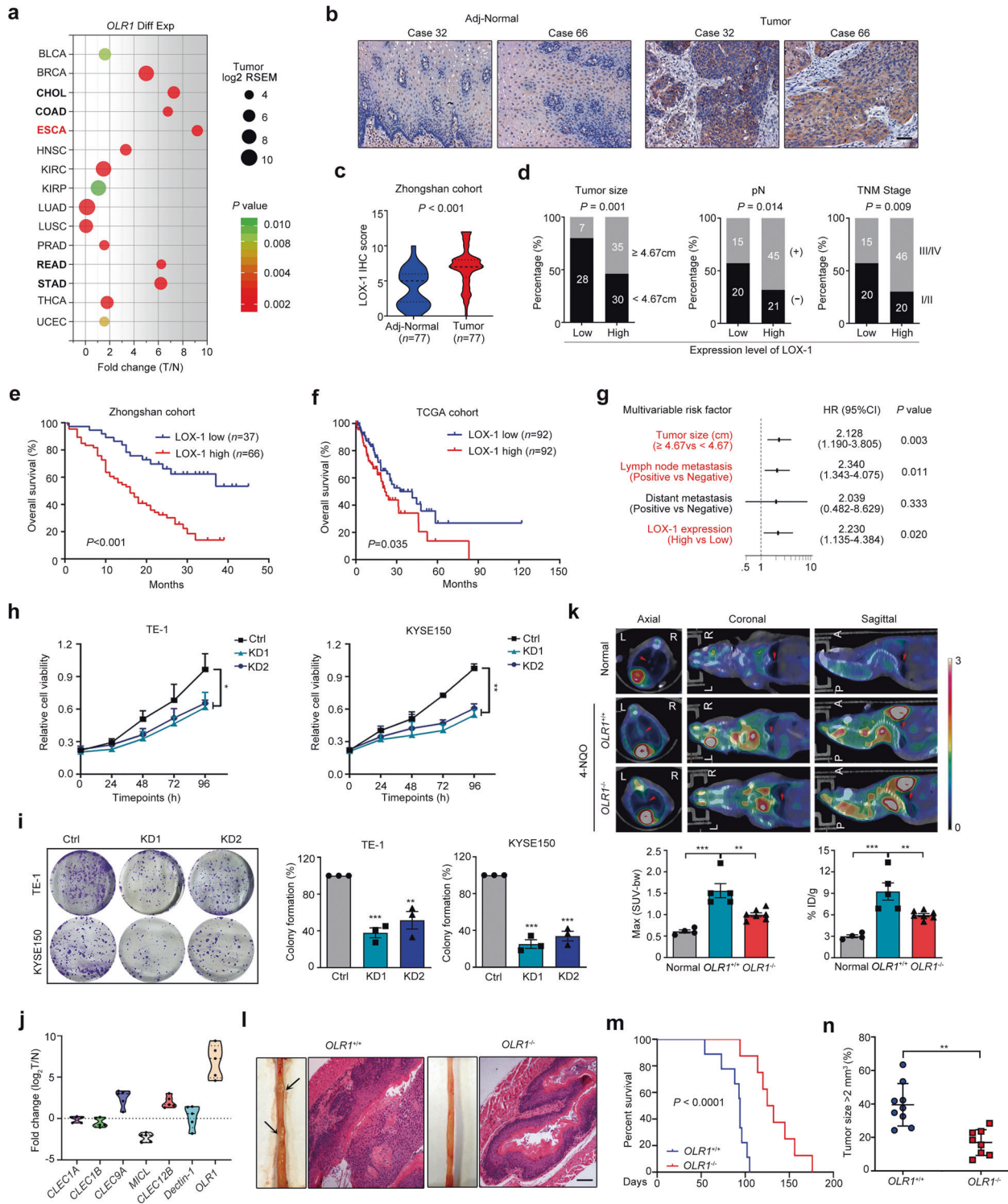
RESULTS

LOX-1 fuels EC development

To explore the expression patterns of LOX-1 in tumor, we analyzed the LOX-1 mRNA profiles from the TCGA database. As shown in Fig. 1a, LOX-1 expression increased in all the tumors of the digestive system, and esophageal carcinoma (ESCA) showed the highest fold change (Fold change = 9.15). Immunohistochemistry (IHC) staining in tissue microarrays further confirmed that LOX-1 protein was overexpressed in EC tissues (Fig. 1b, c). For evaluating

¹NHC Key Laboratory of Glycoconjugate Research, Department of Biochemistry and Molecular Biology, School of Basic Medical Sciences, Fudan University, Shanghai 200032, China. ²Department of General Surgery, Zhongshan Hospital, Fudan University, Shanghai 20032, China. ³Key Laboratory of Marine Drugs of Ministry of Education, Shandong Provincial Key Laboratory of Glycoscience and Glycotechnology, School of Medicine and Pharmacy, Ocean University of China, Qingdao, 266003, China; Laboratory for Marine Drugs and Bioproducts, Pilot National Laboratory for Marine Science and Technology (Qingdao), Qingdao 266237, China. ⁴Institutes of Biomedical Sciences, Shanxi University, Taiyuan 030006, China. ⁵These authors contributed equally: Can Li, Fenglin Liu, Xu Yang. [✉]email: wanglan@fudan.edu.cn
Edited by H-U Simon

Received: 31 May 2021 Revised: 24 September 2021 Accepted: 24 September 2021
Published online: 5 October 2021



the correlation between LOX-1 expression and different clinico-pathologic features in EC patients, all the patients included in this study were divided into two groups according to LOX-1 expression (Fig. S1a). We found the high expression of LOX-1 in EC was strongly associated with larger tumor size, more extensive lymph node metastasis, and later TNM stage (Fig. 1d). Moreover, Kaplan–Meier analysis revealed that the patients with high expression of LOX-1 showed shorter overall survival (OS) (Fig. 1e, f). Univariate Cox regression analysis demonstrated that LOX-1

expression, tumor size, lymph node metastasis, distant metastasis, and TNM stage are risk factors for OS of EC patients (Fig. S1b), and further multivariate analysis showed that LOX-1 expression was an independent prognostic factor for EC (Fig. 1g). Taken together, these results indicate that LOX-1 is overexpressed in EC and correlated with a poor prognosis.

To investigate the tumorigenicity of LOX-1, we transfected siRNA targeting LOX-1 into EC cells (Fig. S2a) and found LOX-1 depletion significantly inhibited cell viability and clonogenicity

Fig. 1 LOX-1 is upregulated in esophageal cancer and its deficiency restrains tumorigenesis. **a** Scatter diagram illustrating *OLR1* expression in various cancers. The abscissa is the fold change value of LOX-1 expression from tumor vs normal. Size represents the mean value of LOX-1 expression in the tumor tissues. The color indicates *P* values. Digestive tract cancers were marked with bold font. **b** Images shown are representative in EC cases (Scale bar, 50 μ m). **c** Quantitative analysis of IHC staining for LOX-1 in esophageal tumor/peritumor samples from Zhongshan cohort (Student's *t*-test). **d** Correlations between LOX-1 expression and tumor size, lymph node metastasis (pN), and TNM stage in Zhongshan cohort (Yates' chi-square test). **e** Kaplan–Meier survival analysis of overall survival in patients from Zhongshan cohort (Log-rank test). **f** Kaplan–Meier survival analysis of overall survival in patients from TCGA cohort (Log-rank test). **g** Multivariate analysis was performed in Zhongshan cohort. The bars correspond to 95% confidence intervals. **h** Cell viability was detected by CCK-8 assay at the indicated time (two-way ANOVA). **i** Colony formation assay of EC cells transfected with LOX-1 siRNA (KD1/KD2) or negative control (Ctrl) for 48 h (Student's *t*-test). **j** Esophageal tumor tissues from 4-NQO induced esophageal cancer (EC) model were collected for RT-qPCR analysis, and the \log_2 values of tumor vs normal were shown (Student's *t*-test, $n = 5$). **k** Representative ^{18}F -FDG PET/CT images and quantification of ^{18}F -FDG signal in regions of interest (ROI) are shown (one-way ANOVA). The red arrow indicates ROI; L left, R right, A anterior, P posterior. Max (SUV-bw), maximum PET SUV from body weight. %ID/g injected dose per gram. **l** Representative images of 4-NQO-induced EC mouse, HE staining of the esophagus (Scale bar, 100 μ m). **m** Kaplan–Meier survival analysis of overall survival in 4-NQO-induced wild-type mice and 4-NQO-induced *OLR1*^{-/-} mice (Log-rank test, $n = 9$). **n** The tumor sizes of 4-NQO-induced wild-type mice and 4-NQO-induced *OLR1*^{-/-} mice (one-way ANOVA, $n = 8$). * $P < 0.05$, ** $P < 0.01$, *** $P < 0.001$.

(Fig. 1h, i). Notably, we found that LOX-1 exhibited the highest expression level among the members of the “Dectin-1 cluster” in the mouse EC tissues of the 4-NQO-induced EC model (Fig. 1j), suggesting that LOX-1 may be a tumor driver. To further explore the role of LOX-1 in vivo, we established the EC model in wild-type mice (hereafter, *OLR1*^{+/+}) and LOX-1 deficient mice (hereafter, *OLR1*^{-/-}). ^{18}F -FDG micro-PET-CT imaging displayed *OLR1*^{-/-} mice with smaller tumor lesions and lower ^{18}F -FDG uptake (Fig. 1k). In addition, hematoxylin-eosin (HE) staining showed that the esophagus of *OLR1*^{+/+} mice were filled with more tumor tissues (Fig. 1l). Importantly, compared to *OLR1*^{-/-} mice, the survival time of *OLR1*^{+/+} mice was decreased and the tumor size was significantly increased (Fig. 1m, n).

LOX-1 knockdown inhibits EC cell growth through autophagy

The acceleration of neoplastic progression is mainly due to deregulated cell proliferation and suppressed cell death [14]. Oddly, flow cytometry analysis demonstrated that LOX-1 deficiency had no effect on cell cycle arrest (Fig. S2b). Further TUNEL labeling and Annexin V/PI double staining indicated that apoptotic or necrotic cells did not increase in the LOX-1 knockdown group (Fig. S2c, d). In addition to apoptosis, programmed cell death also includes autophagic cell death. Further by treating with different inhibitors, we found autophagy inhibitor 3-methyladenine (3-MA) but not apoptosis inhibitor Z-VAD-FMK (zVAD) or necrosis inhibitor Necrostatin-1 (Nec-1) prevented LOX-1 deletion-induced cell viability decline (Fig. 2a). By using transmission electron microscopy (TEM), we observed the nuclei of LOX-1 knockdown cells were intact with a large number of autophagic vacuoles in the cytoplasm, suggesting that autophagy is activated in these cells (Fig. 2b, c). Further immunoblot confirmed that LOX-1 deficiency led to an increased LC3-II and a decreased p62 (Fig. 2d). These results suggest that autophagy is involved in the cell viability regulated by LOX-1.

As LC3-II accumulation is attributed to either increased autophagosome formation or impaired autophagosome-lysosome fusion, the effect of LOX-1 knockdown on LC3-II expression was examined in the presence of chloroquine (CQ), an inhibitor of lysosome that can block autophagosome-lysosome fusion. Of note, we observed that LOX-1 knockdown still increased LC3-II levels in the presence of CQ, while p62 degradation induced by LOX-1 knockdown was blocked by CQ (Fig. 2d), indicating that LOX-1 knockdown enhances autophagosome formation. We next measured the rate of delivery of autophagosomes to lysosomes using the mCherry-GFP-LC3 system. The numbers of autolysosomes and autophagosomes were higher in LOX-1 deleted cells (Fig. 2e, f), suggesting that LOX-1 knockdown promotes the formation of autophagosomes and subsequent fusion with lysosomes.

Loss of LOX-1 incents autophagic program requiring TFEB nuclear translocation

By analyzing the data from TCGA, we found that the LOX-1 expression was negatively correlated with autophagy-lysosome signature genes (Fig. 3a), which was further confirmed in EC tissues from *OLR1*^{-/-} mice (Fig. 3b). Transcription factor EB (TFEB) is a mast autophagy-lysosome regulator by transporting to nuclear to drive expression of a large subset of genes [15, 16]. We questioned whether TFEB was linked to LOX-1 deficiency-induced autophagic cell death. Notably, the percentage of nuclear located TFEB was dramatically increased in LOX-1 knockdown cells (Fig. 3c, d). Substitution of phosphorylate specific serine residues in TFEB may affect nuclear transport by changing the binding affinity for importins or modulating nuclear location signal (NLS) [17]. In parallel, LOX-1 knockdown cells showed reduced TFEB serine phosphorylation (Fig. 3e), raising the possibility that the dephosphorylation and nuclear localization of TFEB is required for LOX-1 knockdown-induced autophagic cell death. To test this, we generated two TFEB mutants (S142D and S211D). Unlike S142D, TFEB S211D was still sufficient to cause TFEB nuclear translocation under LOX-1 depletion (Fig. 3f). Consistently, LOX-1 knockdown-induced colony-forming inhibition activity also occurs in cells with S211D mutants but is very slight in S142D (Fig. 3g). These results suggest that LOX-1 deficiency has an effect on the S142 phosphorylation of TFEB for driving its nuclear translocation.

It has been documented that the decrease of *MAP1LC3B* is accompanied by the levels of TFEB downregulation [15]. We assumed that LOX-1 siRNA may enhance *MAP1LC3B* expression through TFEB dephosphorylation. Indeed, administration of TFEB S142D mutant but not S211D abolished the increased mRNA level of LC3B induced by LOX-1 siRNA (Fig. 3h). Based on the predicted binding sites with JASPAR and chromatin immunoprecipitation (ChIP) assay, DNA from TFEB overexpressing cells showed an obvious enrichment of two specific regions (150 to 159 bp and 1763 to 1772 bp) (Fig. 3i). Only TFEB S142D robustly blocked the upregulated LC3-II and the downregulated p62 induced by LOX-1 deficiency (Fig. 3j). These results confirm that TFEB S142 but not S211 is critical for LOX-1 depletion-induced autophagy in EC. Nuclear TFEB staining was lower in the esophageal specimens from *OLR1*^{+/+} mice than *OLR1*^{-/-} mice (Fig. 3k), showing a clear relation between LOX-1 expression with TFEB nuclear localization.

ERK inhibitor disrupts LOX-1-induced TFEB phosphorylation and tumorigenesis

To clarify the mechanism of LOX-1 modulating TFEB-related autophagy in EC, we screened eight differentially regulated signaling molecules in LOX-1-depleted TE-1 cells by performing a human phosphokinase antibody array, among which phospho-ERK1/2 (T202/Y204) level was significantly decreased (Fig. 4a).

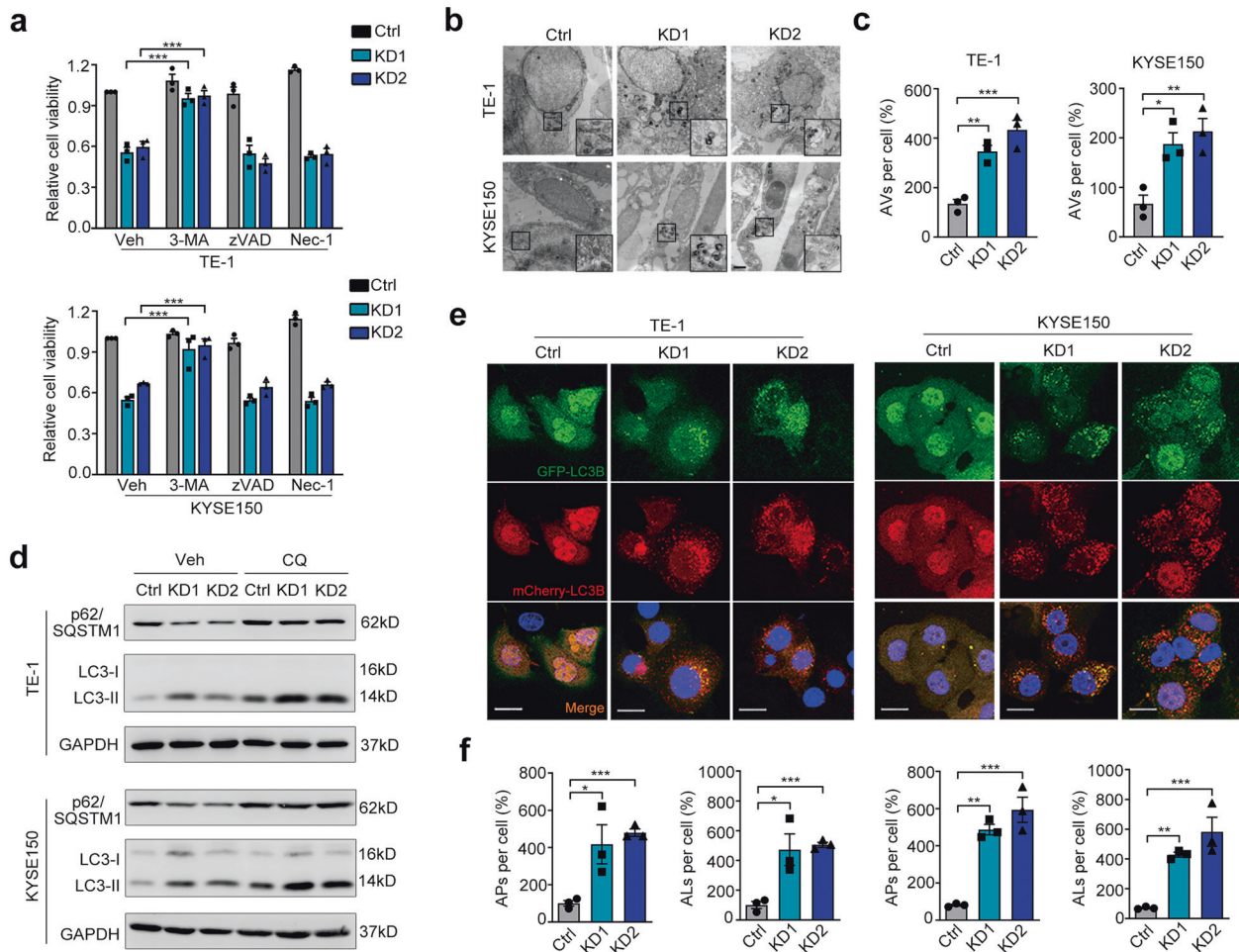


Fig. 2 Autophagic cell death is involved in LOX-1-knockdown mediated tumor inhibition. **a** TE-1 and KYSE150 cells transfected with LOX-1 siRNA or control were treated with 3-methyladenine (3-MA, 200 μM) or Z-VAD-FMK (zVAD, 10 μM) or necrosis inhibitor Nec-1 (10 μM), and cell viability was detected by CCK-8 assay (Student's *t*-test). **b** Ultrastructure of cells transfected with LOX-1 siRNA or control were analyzed by transmission electron microscopy (TEM) (Scale bar, 2 μm). **c** Statistic analysis of autophagic vacuoles (AVs) induced by LOX-1 knockdown (Student's *t*-test). **d** Cells transfected with LOX-1 siRNA or control were treated with lysosome inhibitor chloroquine (CQ, 50 μM) or vehicle (Veh) for 4 h, and the changes of autophagy markers were analyzed by immunoblot. **e** Autophagic flux detection with the mCherry-GFP-LC3 reporter. Cells stably expressing mCherry-GFP-LC3 were transfected with LOX-1 siRNA or control, confocal microscopy images of representative cells were acquired (Scale bars, 20 μm). Blue represents DAPI; APs, mCherry⁺ autophagosomes; ALs, mCherry⁺ GFP⁻ autolysosomes. **f** The percentages of vesicles per cell were calculated (Student's *t*-test). **P* < 0.05, ***P* < 0.01, ****P* < 0.001.

Additionally, GSEA analysis of the TCGA database displayed that the KRAS signaling pathway, a well-known regulator of ERK, was enriched in the LOX-1 overexpression group (Fig. 4b). To determine whether ERK1/2 phosphorylation was essential for LOX-1-mediated EC development, we established constitutively active ERK2 (caERK2) with two mutant points R67S and D321N, which increases ERK2 autophosphorylation in a MEK1/2-independent fashion and renders the kinase insensitive to phosphatases. The biologic events such as ERK1/2 phosphorylation down-regulation, autophagy activation and cell viability suppression induced by LOX-1-knockdown were reversed in caERK2 overexpressed cells (Fig. 4c, d).

Next, we investigated whether ERK signaling was essential for LOX-1 deficient-induced TFEB activation. As shown in Fig. 4e and f, LOX-1 deficient-induced TFEB nuclear transcribing was strongly blocked by caERK2 overexpression. Through monitoring fluorescent photon fluxes in the xenograft mouse model, we found LOX-1 overexpression significantly increased the luminescence intensity, while the enhanced luminescence was abolished after administration of ERK1/2 inhibitor SCH772984 (Fig. 4g, h). Moreover, LOX-1-overexpressed tumors had a significantly increased

growth rate and tumor weight, which were restrained by SCH772984 (Fig. 4i-k). And immunoblot analysis showed that SCH772984 blocked LOX-1 overexpression induced ERK signaling and inhibition of autophagy (Fig. 4l).

Membrane LOX-1 interacts with RACK1 to initial RAS/MEK/ERK signaling and TFEB phosphorylation

LOX-1, as a pattern recognition receptor, regulates the expression of effector genes mainly through signal transduction, while its cytoplasmic tail is very short with only 36 amino acids, and lacks classical signal transduction motifs. To understand LOX-1 induced signal transduction in EC, we performed co-immunoprecipitation and NanoUPLC-nano-ESI-MS/MS analysis in EC cells. A scaffold protein receptor of activated protein C kinase 1 (RACK1) was found to interact with LOX-1 (Fig. 5a), which was confirmed by reciprocal co-immunoprecipitation in HEK293T cells (Fig. 5b). Further in situ proximity ligation assay (PLA) displayed that this interaction occurred in the cytoplasm of EC cells (Fig. 5c). Remarkably, RACK1 silence reversed the activation of MEK-ERK signaling, inhibition of autophagy, and promotion of cell viability induced by LOX-1 overexpression (Fig. 5d, e).

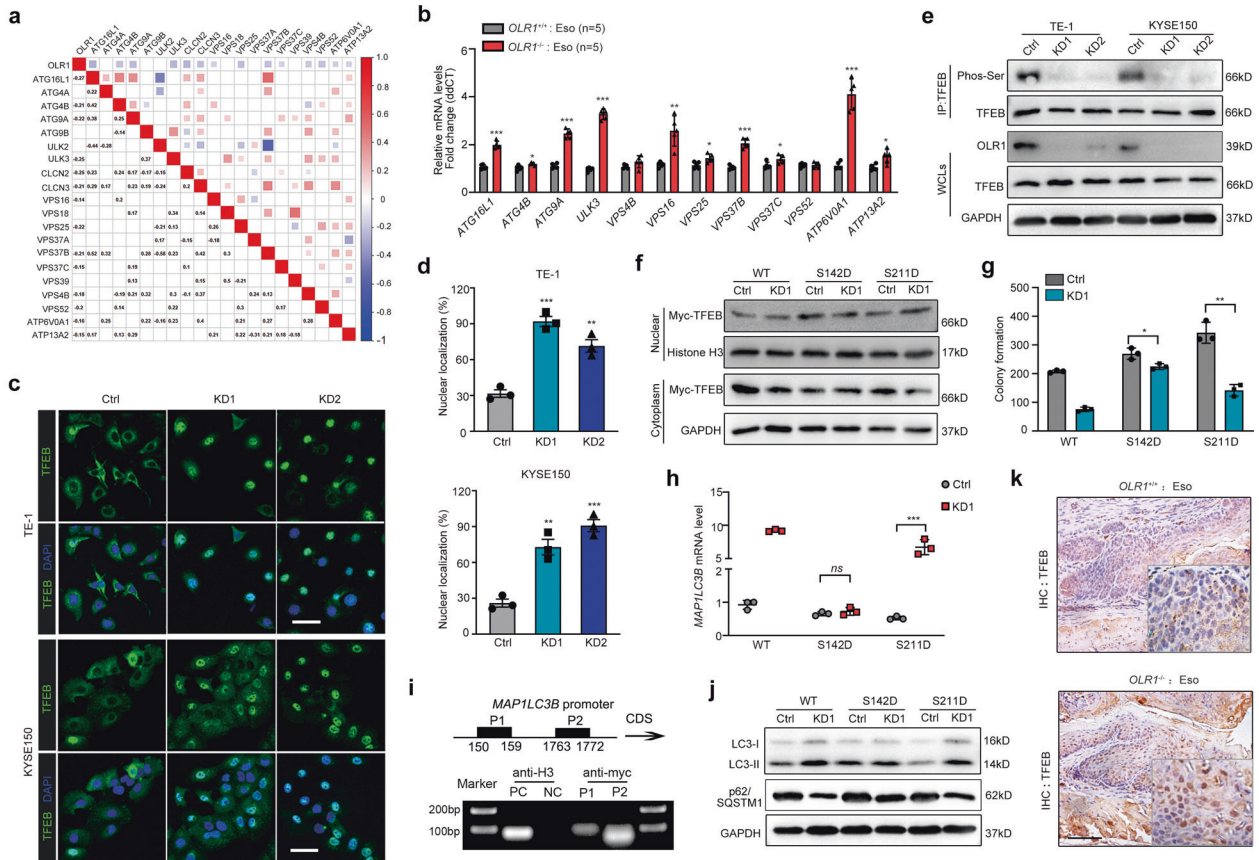


Fig. 3 LOX-1 deletion induces TFEB dephosphorylation and nuclear transport. **a** Correlations Matrix of LOX-1 with autophagy and lysosome-related genes in ESCA tumors of TCGA. **b** RT-qPCR analysis of esophageal tissues from *OLR1*^{+/+} and *OLR1*^{-/-} mice (Student's *t*-test, *n* = 5). **c** Representative confocal images of TFEB (green) in cells transfected with LOX-1 siRNA (Scale bar, 50 μ m). **d** Measurements of TFEB nuclear localization (Student's *t*-test). **e** Immunoprecipitation of cells for TFEB followed by immunoblot for Ser phosphorylation. **f** Immunoblots for Myc-TFEB in the cytoplasmic/nuclear fractions of KYSE150 cells transfected with LOX-1 siRNA or not, which were co-transfected with wild-type TFEB (WT) and TFEB mutants (S142D and S211D). Histone H3 is the control for the nuclear fractions, whereas GAPDH is the control for the cytoplasmic fractions. **g**, **h** Colony formation measurements (**g**) and *MAP1LC3B* mRNA analysis (**h**) of KYSE150 cells transfected with LOX-1 siRNA or not, which were co-transfected with wild-type TFEB (WT) and TFEB mutants (S142D and S211D) (Student's *t*-test). **i** KYSE150 cells were transfected with Myc-TFEB or vector and subjected to CHIP with Myc-tag antibody. Amplificated binding region of TFEB in *MAP1LC3B* promoter was shown by PCR gel. **j** The changes of autophagy and lysosome markers were analyzed by immunoblot in KYSE150 cells. **k** Esophageal tissues from *OLR1*^{+/+} mice and *OLR1*^{-/-} mice were conducted with IHC staining of TFEB (Scale bars, 50 μ m). **P* < 0.05, ***P* < 0.01, ****P* < 0.001, *ns* not significant.

RACK1 can interact with a wide variety of proteins and modulate their stability and activity, including many proteins involved in phosphorylation [18]. Using the STRING database, we found that RACK1 associated with Son of Sevenless 1 (SOS1) (Fig. 5f), a RAS-specific guanine nucleotide exchange factor for activating RAS after being recruited to the plasma membrane [19]. To confirm the predicted result, we performed co-immunoprecipitation in EC cells, and the interaction analysis revealed that RACK1 could form a complex with LOX-1 and SOS1 (Fig. 5g). Of note, through the RAF-RBD pull-down of RAS-GTP, we found that SOS1 silence reversed the increase of activated RAS triggered by LOX-1 (Fig. 5h). Therefore, the inhibitors of the RAS-MEK-ERK pathway may serve as an attractive therapeutic strategy for LOX-1-driven EC.

The results above have shown that the interaction between LOX-1 and RACK1 occurs mainly in the cytoplasm, while the KKxK motif in the cytoplasmic domain (CD) is crucial for LOX-1 surface location [20]. To clarify whether the cytoplasmic or transmembrane form of LOX-1 interacts with RACK1, we constructed LOX-1 mutant (K22/23/25E). Our in situ PLA showed that the interaction between LOX-1 and RACK1 disappeared in LOX-1 mutant transfected cells (Fig. 5i). Further GST-pull-down assay demonstrated a direct interaction between LOX-1 CD and RACK1, which

was vanished in LOX-1 CD with K22/23/25E mutation (Fig. 5j). Of note, overexpressed LOX-1 but not LOX-1 K22/23/25E mutant rescued LOX-1 knockout-induced cell growth inhibition (Fig. 5k). Thus, our results indicate that RACK1 is a necessary partner for the modulation of the function of LOX-1 in RAS-MEK-ERK signaling, autophagy, as well as cell growth, and the KKxK motif decided LOX-1 surface location is crucial for their interaction.

Sulfate polysaccharide fucoidan binds LOX-1 to facilitate LOX-1 degradation

Fucoidan is a sulfated polysaccharide from marine brown algae and has been reported to inhibit ox-LDL-mediated physiological functions [21], which inspires us to explore the relationship between fucoidan and LOX-1 in EC. As shown in Fig. 6a, the surface plasmon resonance (SPR) result suggested fucoidan has a high affinity with LOX-1. Of interest, fucoidan combined with LOX-1 and rapidly reduced its protein expression in EC cells (Fig. 6b), but did not affect the mRNA levels (Fig. S3a). Furthermore, flow cytometry analysis and membrane separation assay revealed that the surface expression of LOX-1 but not cytoplasm expression was downregulated in fucoidan-treated cells (Fig. 6c, d). These results imply that fucoidan decreases the expression of membrane LOX-1 at a posttranscriptional level.

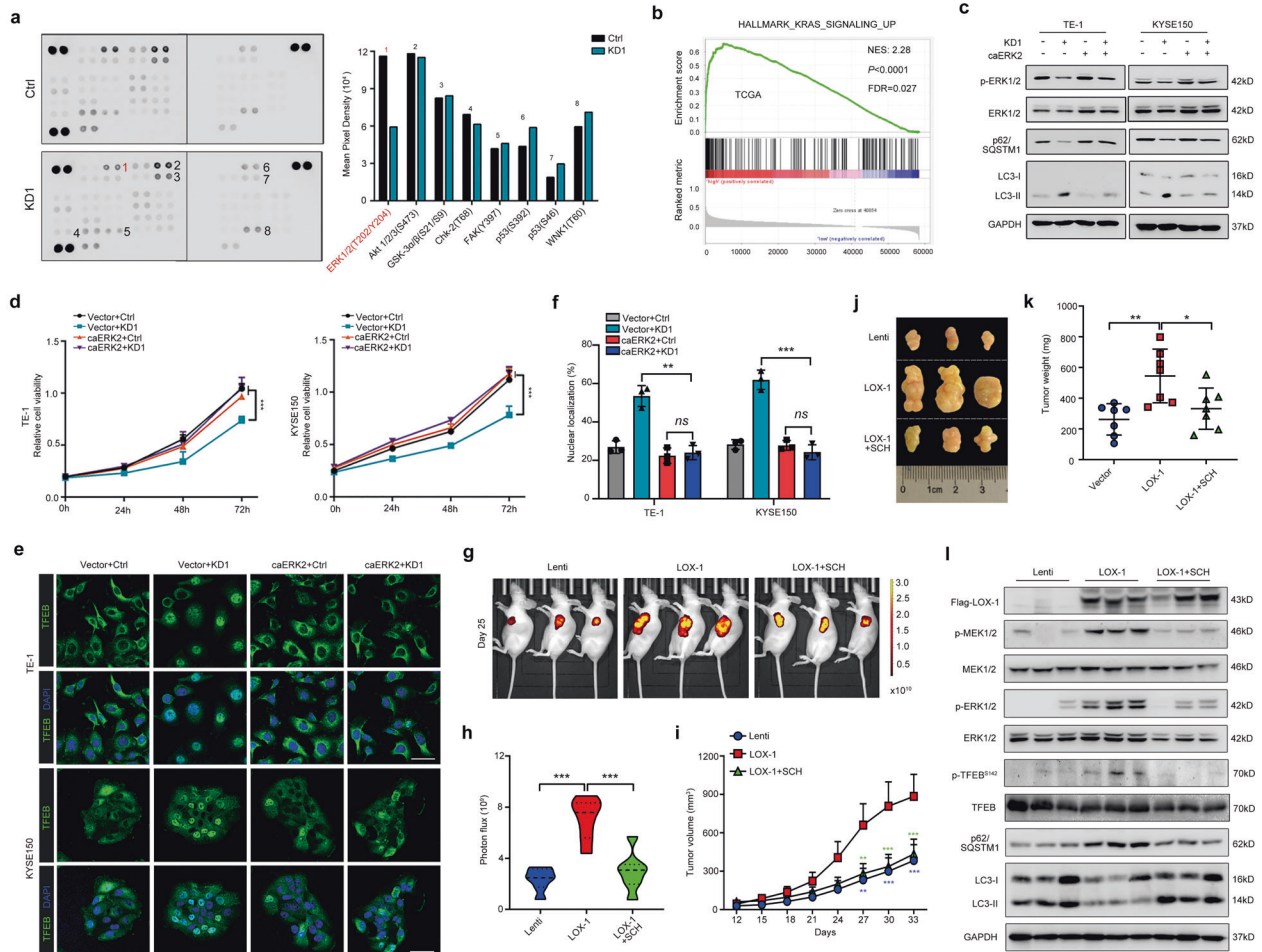


Fig. 4 Disruption of LOX-1 in EC blocks MEK-ERK signaling and induces TFEB nuclear translocation. **a** TE-1 cells transfected with LOX-1 siRNA#1 (KD1) or negative control (Ctrl) were applied to phosphokinase antibody array, and pixel densities of indicated proteins are shown in the right panel. **b** Gene Set Enrichment Analysis (GSEA) about *OLR1* mRNA expression and KRAS signaling gene set in EC databases from TCGA. **c** Cells stably expressing constitutively active ERK2 (caERK2) or empty vector were transfected with KD1 or Ctrl, and immunoblot analysis of p-ERK1/2, ERK1/2, p62, and LC3 was performed. **d** Cells stably expressing caERK2 or empty vector were transfected with KD1 or Ctrl, and cell viability was measured by CCK-8 assay at the indicated time (two-way ANOVA). **e** Cells stably expressing caERK2 or empty vector were transfected with KD1 or Ctrl, and confocal images of representative cells were acquired (Scale bar, 50 μ m). **f** Statistical analysis of TFEB nuclear translocation (Student's *t*-test). **g**, **h** KYSE150 cells stably expressing Flag-LOX-1-GFP (LOX-1) or GFP control (Lenti) were injected into the left flank of nude mice and followed by treatment with vehicle or SCH772984 (SCH, 25 mg/kg) (one-way ANOVA, $n = 7$). Representative images (**g**) and statistical data of photon fluxes (**h**). **i** Tumor growth curves of nude mice are shown as indicated (two-way ANOVA). **j**, **k** Representative images of tumors (**j**) and statistical analysis of weights (**k**) in mice were shown under different conditions. **l** Tumor tissues from xenografts were detected with protein expression of indicated genes by immunoblot analysis. * $P < 0.05$, ** $P < 0.01$, *** $P < 0.001$.

By using de novo protein synthesis inhibitor cycloheximide (CHX), we found that the half-life of LOX-1 was much shorter in EC cells exposed to fucoidan (Fig. 6e). In eukaryotic cells, the lysosome degradation mechanism and ubiquitin-labeled protein degradation pathway are the main systems for protein degradation [22]. Further study showed that proteasome inhibitor MG132 but not lysosome inhibitor CQ blocked fucoidan-induced LOX-1 degradation (Fig. 6f). Moreover, fucoidan increased ubiquitination of LOX-1 in EC cells and HEK293T cells (Fig. 6g), indicating a ubiquitin-related proteasome degradation of LOX-1 is induced by fucoidan. To better understand the potential binding model between fucoidan and LOX-1, molecular docking studies were performed using the Glide model from Schrödinger software. The 3D binding model showed a nice interaction between the dimer of fucoidan and LOX-1 CTLD, and the 2D binding model showed that the primary interactions of fucoidan with LOX-1 CTLD were through the formation of force like H-bond and salt bridge (Fig. 6h). The data above suggest that fucoidan directly binds to

LOX-1 and induces LOX-1 to undergo ubiquitination-mediated proteasomal degradation.

Fucoidan blockade with LOX-1 confers to an autophagic vulnerability and tumorigenic repression in 4-NQO-induced EC

Considering fucoidan induces LOX-1 degradation, we next investigated the role of fucoidan in the downstream effective events of LOX-1. The activity analysis revealed that fucoidan led to a suppressive tumor growth ex vivo and in vivo (Fig. S3b–d). Additionally, characteristics and signals of autophagy were also observed in the fucoidan-treated cells (Fig. S3e, f and Fig. 7a), and autophagy inhibitor rescued fucoidan-induced EC cell death (Fig. 7b). By administrating fucoidan to the wild EC cells and LOX-1 silencing cells separately, cell viability inhibition was detected and the data showed that loss of LOX-1 effectively reduced the inhibition of fucoidan in cell growth (Fig. 7c). We further constructed a 4-NQO induced EC model in *OLR1*^{-/-} mice

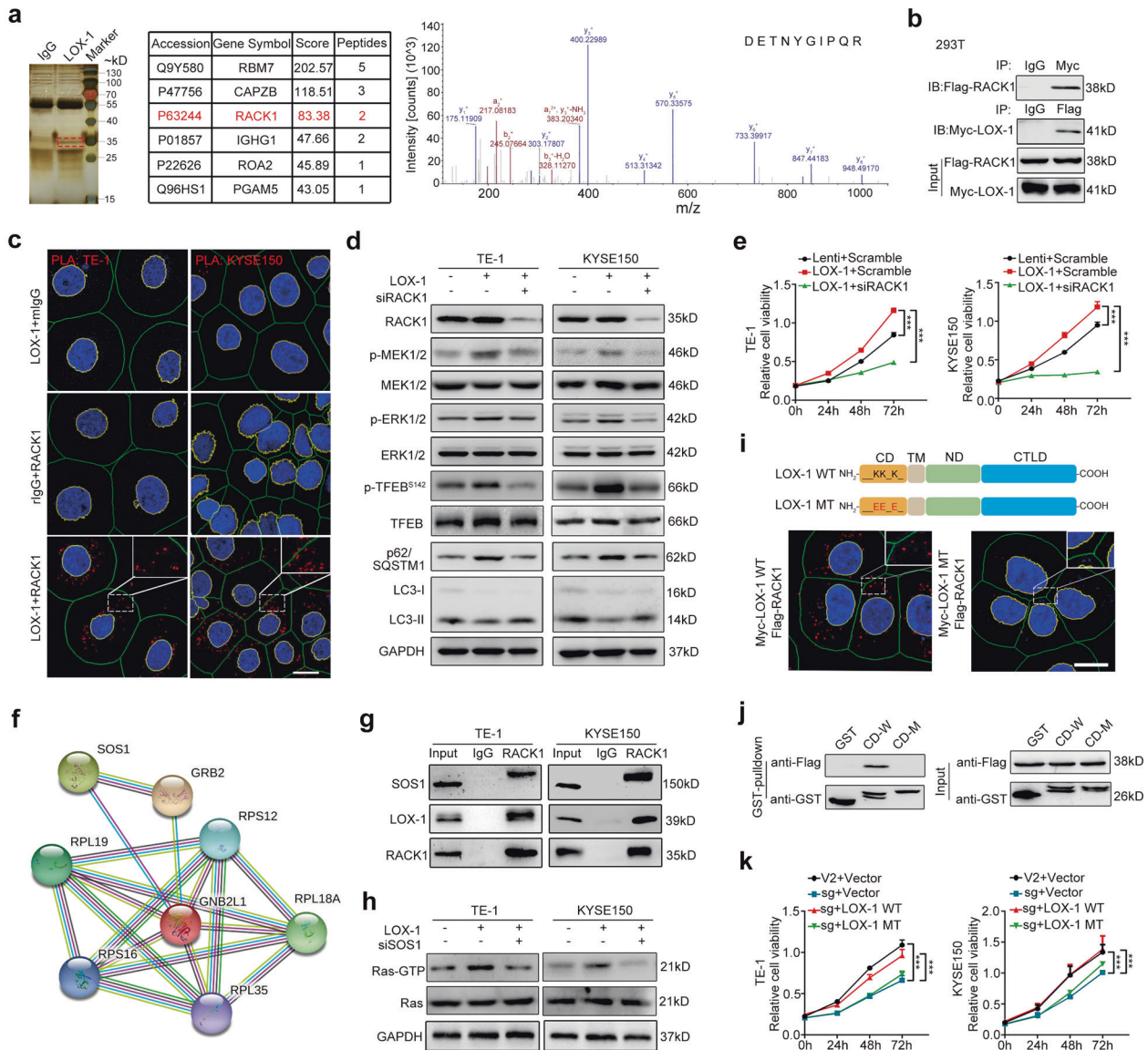


Fig. 5 RACK1 binds membrane LOX-1 to regulate RAS/MEK/ERK signaling pathway and autophagic cell death. **a** Identification of RACK1 as LOX-1-associated protein by mass spectrogram analysis in TE-1 cells. A representative peptide of RACK1 is shown. **b** Co-IP analysis in HEK293T cells co-transfected with Myc-LOX-1 and Flag-RACK1 plasmids. **c** In situ PLA was performed on EC cells. Blue represents DAPI, and red fluorescence represents LOX-1-RACK1 interactions (Scale bars, 20 μ m). **d** Cells stably expressing LOX-1 or not were transfected with siRACK1 or control, and immunoblot analysis of key elements expression involved in MEK-ERK signaling and autophagy pathway was performed. **e** Cells stably expressing Flag-LOX-1-GFP (LOX-1) or GFP control (Lenti) were transfected with RACK1 siRNA (siRACK1) or scramble siRNA, and subjected to CCK-8 assays (two-way ANOVA). **f** STRING interaction diagram of RACK1 with other proteins. **g** Co-IP of LOX-1, RACK1, and SOS1 in EC cells. **h** Ras activity were determined by a Ras-GTP pull-down assay, and cell lysates were subjected to immunoblot analysis of GAPDH. **i** Schematic representation of Myc-tagged wild type (LOX-1-WT) and point mutation constructs (LOX-1 MT) of human full-length LOX-1 (top). The interaction between Myc-LOX-1-WT/MT and Flag-RACK1 was determined by in situ PLA in HEK293T cells co-transfected with indicated plasmids (bottom). Blue represents DAPI, and red fluorescence represents RACK1-LOX-1 interactions (Scale bar, 20 μ m). **j** The interactions of RACK1 and GST-tagged wild-type (CD-W) or point mutation constructs (CD-M) of the cytoplasmic domain of LOX-1 were determined by GST pull-down assay. **k** Cells with LOX-1 knockout using CRISPR-sgLOX-1 system (sg) or not (V2) were transfected with LOX-1-WT or LOX-1-MT or empty vector, and cell viability was measured by CCK-8 assay at the indicated time (two-way ANOVA). *** $P < 0.001$.

to determine the anticarcinogenic effect of fucoidan in *OLR1* knockout mice (Fig. 7d). There were no quantitative changes in tumor sizes, body weight, and survival time of fucoidan-treated *OLR1*^{-/-} mice, while the decreased tumor sizes, improved body weight, and extended survival time were observed in fucoidan-treated wild-type mice (Fig. 7e–g). By performing IHC staining on the esophageal tumor tissues from the mice with different treatments, we found p-ERK1/2, p-TFEB, and p62 levels were diminished synergistically in the tumor tissues of fucoidan-treated *OLR1*^{+/-} group, while there were no differences between the

tumor tissues of fucoidan-treated and saline-treated *OLR1*^{-/-} group (Fig. 7h, i). Altogether, these data indicate that blockade of LOX-1 by fucoidan suppresses esophageal carcinogenesis with increased autophagic activity.

LOX-1 deletion suppresses angiogenesis and immune cells infiltration in EC

LOX-1 activation has been reported to induce pro-inflammatory and pro-angiogenic roles [23, 24]. Although these biological effects were studied in vitro or in the context of atherosclerosis

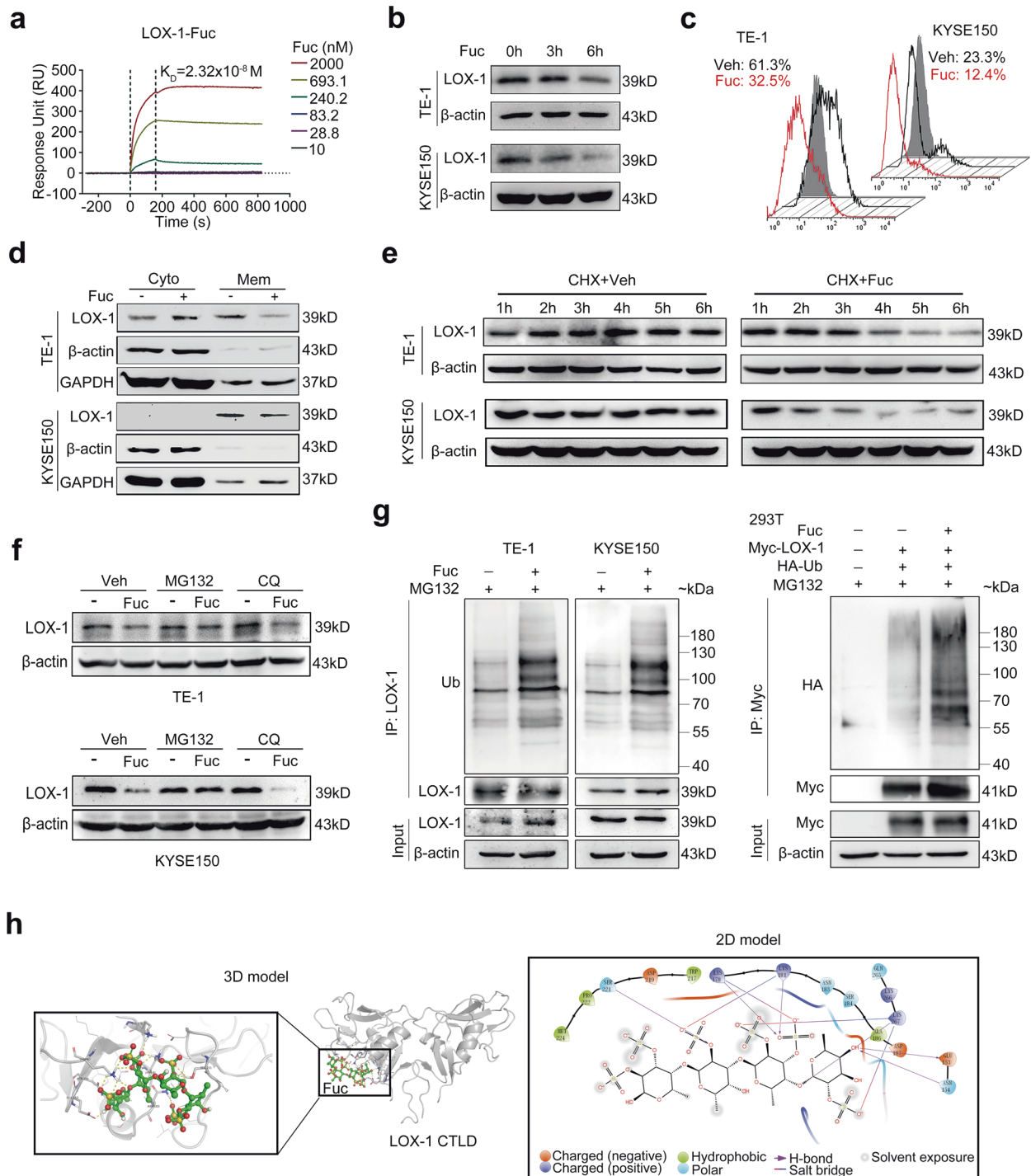


Fig. 6 Fucoidan induces ubiquitin-mediated degradation of LOX-1. **a** Sensorgram for the interaction of different amounts of fucoidan (Fuc) with immobilized human recombinant protein of LOX-1 C-type lectin-like domain (LOX-1-CTLD) obtained from surface plasmon resonance (SPR) analysis. **b** Immunoblot analysis of LOX-1 expression in cells treated with fucoidan (200 $\mu\text{g}/\text{mL}$) at the indicated time. **c** Flow cytometry analysis of LOX-1 expression. **d** Cell surface expression of LOX-1 in cells treated with fucoidan (200 $\mu\text{g}/\text{mL}$) or vehicle (Veh) for 6 h was examined by membrane separation assay. **e** Time-course studies of LOX-1 degradation. EC cells were treated with cycloheximide (CHX) in the presence or absence of fucoidan (200 $\mu\text{g}/\text{mL}$) and followed by immunoblot analysis. **f** Immunoblot analysis of LOX-1 expression in EC cells treated with fucoidan in the presence of MG132 (10 μM) or CQ (50 μM). **g** Cells were treated with MG132 (10 μM) for 2 h followed by fucoidan (200 $\mu\text{g}/\text{mL}$) for another 4 h, and lysates were immunoprecipitated with anti-LOX-1 or anti-Myc antibody. **h** Molecular docking of fucoidan and LOX-1 CTLD was performed using the Glide model from Schrödinger software.

and associated vascular diseases, they were very important for tumor development. GSEA results from the TCGA dataset displayed that angiogenesis and inflammatory response gene sets were enriched in LOX-1 high expression phenotype (Fig. S4a,

b). In addition, IHC staining results showed that CD31 and CD45 positive cells were dramatically decreased in EC tissues from *OLR1*^{-/-} group (Fig. S4c). To gain further insight into immune cell responses involved in EC-related LOX-1 regulatory network, we

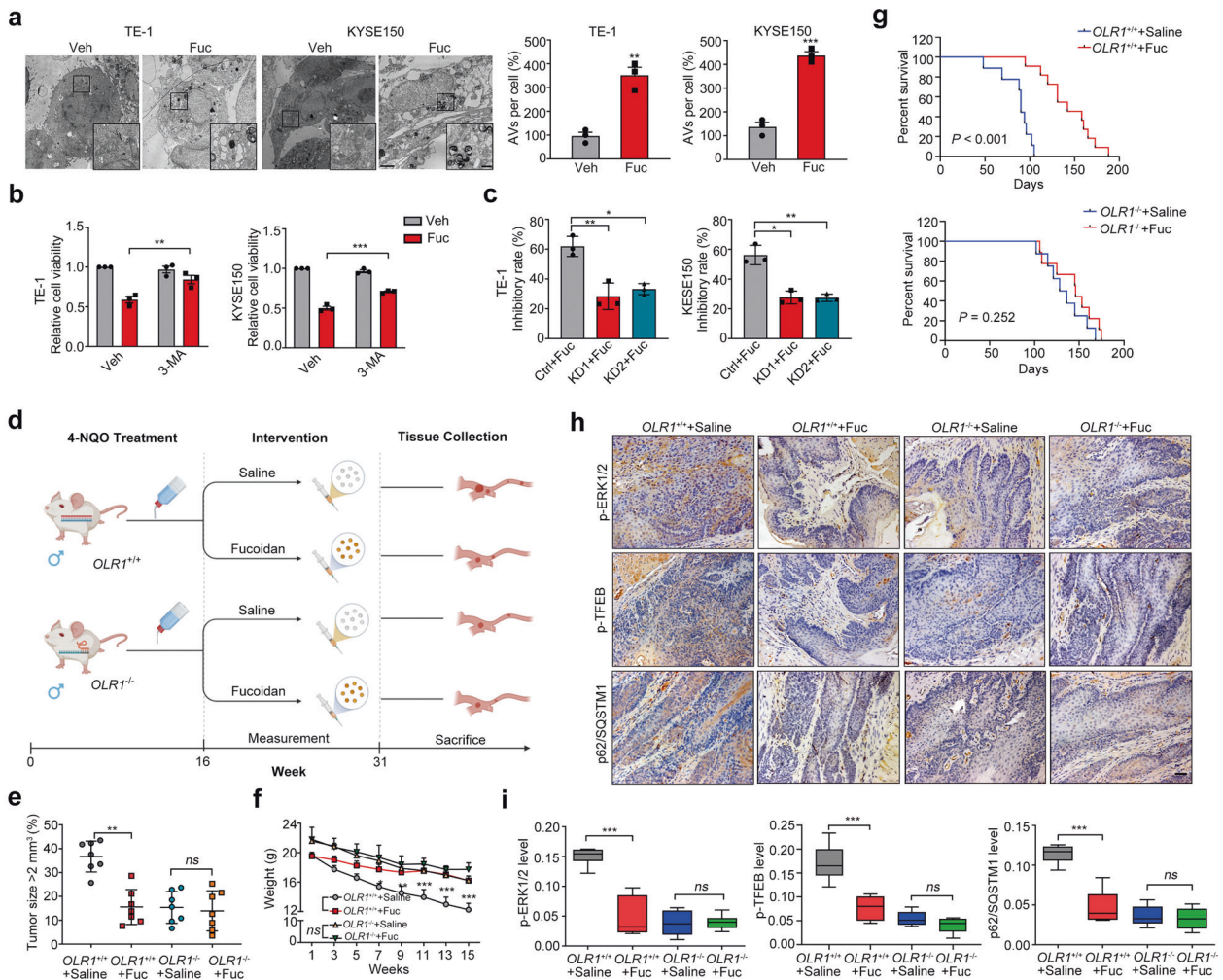


Fig. 7 Mitigation of esophageal tumorigenesis by blockade of LOX-1 with fucoidan. **a** TEM analysis of cells treated with fucoidan (200 $\mu\text{g}/\text{mL}$) for 48 h (Scale bar, 2 μm ; magnification, 500 nm) (Student's *t*-test). **b** Cell viability of cells treated with fucoidan (200 $\mu\text{g}/\text{mL}$) in the presence of 3-MA (200 μM) for 48 h was measured by using the CCK-8 assay (Student's *t*-test). **c** Cells transfected with LOX-1 siRNA (KD1/KD2) or negative control (Ctrl) were treated with fucoidan (200 $\mu\text{g}/\text{mL}$) for 48 h, and cell viability was measured by using the CCK-8 assay (Student's *t*-test). **d** Experiment schematic of 4-NQO-induced genetic mice following treated with saline or fucoidan (Fuc) interference. **e** The tumor sizes of 4-NQO-induced wild-type mice and *OLR1*^{-/-} mice treated with saline or Fuc ($n = 7$, two-way ANOVA). **f** The body weight of 4-NQO-induced genetic mice treated with saline or fucoidan ($n = 7$, two-way ANOVA). **g** Kaplan–Meier survival analysis of overall survival in 4-NQO-induced wild-type mice and *OLR1*^{-/-} mice treated with saline or Fuc (Log-rank test). **h, i** Esophageal tumor tissues from 4-NQO-induced wild-type mice and *OLR1*^{-/-} mice treated with saline or Fuc were conducted with IHC staining of p-ERK1/2, p-TFEB, and p62 (Scale bars, 50 μm), and the representative images and statistical analysis are shown ($n = 7$, student's *t*-test). * $P < 0.05$, ** $P < 0.01$, *** $P < 0.001$, *ns* not significant.

conducted TIMER [25] analysis and found that immune cells, including dendritic cell, macrophage, neutrophil, and CD8⁺ T cell were positively correlated with LOX-1 expression (Fig. S4d). Therefore, the blockade of LOX-1 is possible to diminish tumor angiogenesis and immune cells infiltration in EC.

In conclusion, we demonstrated here that LOX-1 modulated the RAS-MEK-ERK signaling pathway to retain TFEB inactive within cytosol through interacting with RACK1 in EC cells, and the ubiquitin-proteasomal degradation of LOX-1 induced by fucoidan, resulted in prolonged and sustained activation of autophagy to inhibit EC development (Fig. S5, proposed model).

DISCUSSION

Over the decades, researchers were almost focused on the role of LOX-1 expressed in endothelial cells and its participation in the initiation of atherosclerosis. Recently, a series of studies have demonstrated LOX-1 has a positive expression in tumor cells derived from epithelial tissues [26, 27], indicating a potential role

of LOX-1 in modulating epithelial cellular transformation. As one of the most aggressive malignancies, the main treatment of EC except for surgery, chemotherapy, or chemoradiotherapy is the combination of targeted therapies [28, 29]. Of note, to date, the main drugs used clinically for EC is targeting to HER2, which limits to be effective for the patients with HER2 positive [30]. In our study, we found that LOX-1 was overexpressed in EC tissues and served as an independent prognosis factor of EC patients.

Autophagy remains controversial for its dual roles in cancer although significant progress has been made over the past decades [31]. Clarifying the roles of autophagy in specific cancer circumstances could help to develop clinically relevant autophagy drug for effective therapy. Our study revealed that LOX-1 orchestrates phosphorylation of RAS-MEK-ERK, TFEB nuclear translocation, and autophagic network to control EC cell growth. It is interesting that hyperactivation of autophagy plays an essential role in cell death during tumor replicative crisis, providing new insight into the telomere-driven autophagy pathway [32]. Considering that almost all cancer cells have short

telomeres although the activity of telomerase is upregulated [33], autophagy induced by telomere dysfunction may be responsible for keeping cancer cells in balance in a period where cell growth and death. Here in our study, activation of autophagy has been shown to induce cell death in EC, which may be due to the break of balance maintained in cancer cells.

LOX-1 can bind to a broad spectrum of structurally distinct ligands with high affinity, such as ox-LDL, AGEs, CRP, HSP70, and bacterial products, and most of these ligands act to upregulate LOX-1 expression and activate the LOX-1 signaling pathway [12]. Fucoidan is a complex sulfated polysaccharide derived from brown algae that mainly consists of sulfated fucose residues [34] and affects many pathophysiological processes [35]. Previous researches have been reported that fucoidan could inhibit the stimulation of MAPK induced by ox-LDL [21], raising the possibility that fucoidan may competitively bind with LOX-1. Here we confirmed fucoidan is an exogenous ligand of LOX-1 that binds to LOX-1 CTLD directly. LOX-1 as a membrane receptor cycles between the plasma membrane and endosomes independent on the presence of ligand, and traffic to the lysosome for degradation when it is combined with ox-LDL in tripeptide conserved motif (DDL) and the dynamin-2-dependent way [36]. In this study, we found that fucoidan induces ubiquitination-proteasome system-mediated degradation of LOX-1, providing a new insight to understand various pathways below ligand–receptor interaction. Of course, as a scavenger receptor, LOX-1 may also mediate fucoidan endocytosis, and the detailed process of LOX-1-mediated fucoidan internalization, trafficking, and disposition needs to be investigated in further studies.

The degradation products of autophagy provide substrates for both biosynthesis and energy generation [37]. Our results reveal that LOX-1 deficiency initiates autophagic program in EC, suggesting a potential role of LOX-1 in mediating energy metabolism. Moreover, gene set enrichment analysis revealed that LOX-1 is significantly related with KRAS pathway. KRAS, together with other RAS isoforms, represents the most prevalent oncogene in human cancers, yet decades long efforts in the discovery of RAS targeted therapies failed to obtain clinically approved drugs [38, 39]. The relationship between LOX-1 and KRAS and the function of LOX-1 in KRAS mutant tumor such as the modulation of the immune system, are worthy to give more consideration.

MATERIALS AND METHODS

Cell lines and reagents

Cells were maintained at 37 °C in a humidified incubator with 5% CO₂. The human EC cell lines TE-1 and KYSE150 were cultured in RPMI-1640 (Sigma-Aldrich, St Louis, MO, USA) supplemented with 10% FBS (Gibco, Grand Island, NY, USA) and 1× penicillin-streptomycin (Genebase Gene-Tech Co. Ltd, Shanghai, China), and human HEK293T cells were cultured in DMEM (Sigma-Aldrich, St Louis, MO, USA) supplemented with 10% FBS and 1× penicillin-streptomycin. All the cell lines were purchased from Cell Bank of Academia Sinica (Shanghai, China). The cells were authenticated and identified no mycoplasma contamination. The information on all primary antibodies, chemicals, recombinant proteins, critical commercial assays, experimental models, oligonucleotides, recombinant DNA and lentivirus, and software is listed in Table S1.

Patients and clinical specimens

For tissue microarray detection, 77 pairs of esophageal tumor/peritumor tissues and additional 26 tumor tissues were collected from 103 EC patients who underwent surgery at the Department of General Surgery, Zhongshan Hospital (Fudan University, Shanghai, China). All the selected patients were consecutively enrolled if they met the criterion of having pathologically proven EC. The patients were excluded if they had other malignant tumors before, or histories of adjuvant or neo-adjuvant therapies including targeted therapies. Informed consent on the use of clinical specimens was obtained from all patients. The study was authorized by the Ethics

Committee of Basic Medical College of Fudan University. All patients gave written informed consent before participation in this study.

Immunohistochemistry (IHC) staining and evaluation

The human tissue microarrays or mouse esophageal tissue slides were constructed from formalin-fixed, paraffin-embedded specimens, and LOX-1 IHC staining was performed according to UltraVision Quanto Detection protocols. The photographs were obtained by Nikon eclipse Ti-s microscope (Tokyo, Japan). Briefly, intensity score with 0 to 3 and frequency score with 0 to 4 were measured based on staining intensity and heterogeneity of staining, respectively. Composite expression score (CES) calculated from intensity score and frequency score with a full range from 0 to 12 was performed to show the staining intensity and frequency of positive cells. As shown in Fig. S1a, the optimal cutoff value of CES is 7 (CES 7), and CES <7 indicated low LOX-1 expression, while CES ≥7 indicated high expression of LOX-1.

RNA extraction, reverse transcription, and quantitative PCR (RT-qPCR)

Briefly, the total RNA of mouse esophageal tissue or cancer cells was isolated using the TRIzol Reagent (Invitrogen) according to the manufacturer's protocol. One microgram of total RNA was reverse-transcribed using the PrimeScript™ RT reagent Kit with gDNA Eraser. qPCR was performed at StepOnePlus™ Real-Time PCR System (Applied Biosystems) using SYBR Premix Ex Taq™ agent. Primers are listed in Table S2.

Immunoprecipitation and immunoblot

For immunoprecipitation assay, the cells were solubilized with immunoprecipitation buffer (50 mM Tris-HCl pH7.5, 150 mM NaCl, 0.1% NP-40, 15 mM MgCl₂, and 5 mM EDTA), equal amounts of protein were incubated with specific antibody immobilized onto Protein A/G Magnetic Beads (MedChem Express, New Jersey, USA) for 2 h at 4 °C with gentle rotation. Beads were washed extensively with immunoprecipitation lysis buffer and boiled. Protein samples were separated by SDS-polyacrylamide gel electrophoresis, transferred onto polyvinylidene difluoride membranes (Millipore Corp), and incubated with primary antibodies, followed by incubation with horseradish peroxidase (HRP)-conjugated anti-mouse or anti-rabbit secondary antibody (Santa Cruz Biotechnology, Santa Cruz, CA). The immunoreactive proteins were visualized by using a Pro-light HRP chemiluminescence detection kit (Tiangen Biotech, Beijing, China) and the image analyzer Tanon-5200 (Tanon, Shanghai, China).

Transmission electron microscopy (TEM)

Cells were treated as indicated and fixed with 2.5% glutaraldehyde containing 0.1 mol/L sodium cacodylate. Samples were postfixed using 1% osmium tetroxide, followed by dehydration with an increasing concentration gradient of ethanol and propylene oxide. Samples were then embedded, cut into 70 nm sections, and counterstained with 3% uranyl acetate and lead citrate. Images were acquired using a Philips CM120 TEM (Philips, Netherlands) with a cooled CCD camera.

Establishment of ESCA mice model

A stock solution (5 mg/mL) of the carcinogenic 4-NQO was prepared weekly in propylene glycol and diluted in the drinking water to a working concentration of 100 µg/mL. Wild-type C57BL/6 or *OLR1* knockout mice (Cyagen Biosciences) were given drinking water containing 4-NQO for 16 weeks. Then some mice were sacrificed to analyze the lesions in the esophagus, and the rest of the mice were randomly assigned to four groups with different treatments. The body weights, survival time, and general behavioral abnormalities were monitored daily. After 15 weeks, all of the mice were sacrificed, and the esophagus were collected for further analysis. All experimental procedures were performed in accordance with the ethical regulations and approved by the Animal Care and Use Committee of Fudan University.

Immunofluorescence and confocal imaging

Cells seeded on coverslips were washed twice with cold PBS, fixed with 4% PFA at room temperature (RT) for 15 min followed by permeabilization with 0.1% Triton X-100/PBS for 5 min on ice. After incubation in blocking solution (10% BSA/PBS) at RT for 1 h, cells were incubated with primary antibody at 4 °C overnight. Cells were washed in PBS three times and then

incubated with secondary antibodies labeled with Alexa-488 or -549 (Jackson Laboratories, Bar Harbor, ME) for 1 h at RT. For nuclear labeling, cells were incubated with 5 µg/mL DAPI (Beyotime Institute of Biotechnology, Jiangsu, China) for 2 min at RT. After cells were washed with PBS three times, the coverslips were mounted onto glass slides using VECTASHIELD Antifade Mounting Medium (Vector Labs, Peterborough, UK). The fluorescent images were captured using a confocal laser scanning microscope (SP5, Leica, Wetzlar, Germany).

In situ proximity ligation assay (PLA)

PLA was performed using Duolink[®] PLA Fluorescence detection following the manufacturer's protocol. Briefly, cells seeded on coverslips were washed twice with cold PBS, fixed with 4% PFA for 15 min followed by permeabilization with 0.1% Triton X-100/PBS for 5 min. Cells were blocked with Duolink[®] Blocking Solution for 60 min at 37 °C, then incubated with primary antibodies overnight at 4 °C. After conjugating with a pair of oligonucleotide probes (DUO92002 and DUO92004, Sigma-Aldrich), the coverslips were mounted using in situ Mounting Medium with DAPI (DUO82040, Sigma-Aldrich). The fluorescent images were captured using a confocal laser scanning microscope (SP5, Leica).

Small-animal PET/CT imaging of tumor

The wild type and *LOX-1*^{-/-} mice were given drinking water containing 4-NQO for 16 weeks and normal drinking water for additional 8 weeks, then esophageal tumors were detected using PET/CT. Briefly, each mouse was injected with 3.767–4.737 MBq of 2-deoxy-2-[F-18]fluoro-D-glucose (¹⁸F-FDG) via the tail vein 60 min before the PET scan, which was performed on an Inveon system (Siemens Medical Solutions Inc.) located in the Fudan university shanghai cancer center. All the mice underwent micro-CT imaging for anatomic registration following micro-PET imaging. The mean radioactivity concentration within the tumor or organ was obtained from the mean pixel values within the multiple regions of interest (ROI) volumes and was expressed as the standardized uptake value. The standard tracer uptake value (SUV) and injected dose per gram (%ID/g) from the system was calculated to represent the tumor lesion and for statistical comparisons.

Statistical analysis

All studies were performed on at least three independent occasions, expressed as the mean ± SEM unless otherwise indicated. Statistical analyses were performed with SPSS 22.0 and GraphPad Prism software. ROC was used to determine the optimal cutoff value for CES. Pearson's chi-squared test and Yates's correction for continuity test were applied for categorical variables. Continuous variables were analyzed by the Student's *t*-test, one-way ANOVA, or two-way ANOVA test. Survival and univariate analysis were determined by Kaplan–Meier analysis, and statistical analysis was calculated with the log-rank test. The Cox proportional hazards regression model was applied to multivariate analysis. All statistical analyses were two-sided, and *P* value <0.05 was considered statistically significant.

DATA AVAILABILITY

All data associated with this study are present in the paper or the Supplementary Materials.

REFERENCES

- Bray F, Ferlay J, Soerjomataram I, Siegel RL, Torre LA, Jemal A. Global cancer statistics 2018: GLOBOCAN estimates of incidence and mortality worldwide for 36 cancers in 185 countries. *CA Cancer J Clin.* 2018;68:394–424.
- Bollschweiler E, Plum P, Monig SP, Holscher AH. Current and future treatment options for esophageal cancer in the elderly. *Expert Opin Pharmacother.* 2017;18:1001–10.
- Frankell AM, Jammula S, Li X, Contino G, Killcoyne S, Abbas S, et al. The landscape of selection in 551 esophageal adenocarcinomas defines genomic biomarkers for the clinic. *Nat Genet.* 2019;51:506–16.
- Klionsky DJ. Autophagy: from phenomenology to molecular understanding in less than a decade. *Nat Rev Mol Cell Biol.* 2007;8:931–7.
- Amaravadi R, Kimmelman AC, White E. Recent insights into the function of autophagy in cancer. *Genes Dev.* 2016;30:1913–30.
- Yu T, Guo F, Yu Y, Sun T, Ma D, Han J, et al. *Fusobacterium nucleatum* promotes chemoresistance to colorectal cancer by modulating autophagy. *Cell.* 2017;170:548–63 e516.

- Wang P, Zhang J, Zhang L, Zhu Z, Fan J, Chen L, et al. MicroRNA 23b regulates autophagy associated with radioresistance of pancreatic cancer cells. *Gastroenterology.* 2013;145:1133–43 e1112.
- Wang WJ, Wang Y, Chen HZ, Xing YZ, Li FW, Zhang Q, et al. Orphan nuclear receptor TR3 acts in autophagic cell death via mitochondrial signaling pathway. *Nat Chem Biol.* 2014;10:133–40.
- Elgendy M, Sheridan C, Brumatti G, Martin SJ. Oncogenic Ras-induced expression of Noxa and Beclin-1 promotes autophagic cell death and limits clonogenic survival. *Mol cell.* 2011;42:23–35.
- Zelensky AN, Gready JE. The C-type lectin-like domain superfamily. *FEBS J.* 2005;272:6179–217.
- Tone K, Stappers MHT, Willment JA, Brown GD. C-type lectin receptors of the Dectin-1 cluster: physiological roles and involvement in disease. *Eur J Immunol.* 2019;49:2127–33.
- Tian K, Ogura S, Little PJ, Xu SW, Sawamura T. Targeting LOX-1 in atherosclerosis and vasculopathy: current knowledge and future perspectives. *Ann N Y Acad Sci.* 2018;1443:34–53.
- Ding Z, Wang X, Schnackenberg L, Khaidakov M, Liu S, Singla S, et al. Regulation of autophagy and apoptosis in response to ox-LDL in vascular smooth muscle cells, and the modulatory effects of the microRNA hsa-let-7 g. *Int J Cardiol.* 2013;168:1378–85.
- Evan GI, Vousden KH. Proliferation, cell cycle and apoptosis in cancer. *Nature.* 2001;411:342–8.
- Settembre C, Di Malta C, Polito VA, Garcia Arencibia M, Vetrini F, Erdin S, et al. TFEB links autophagy to lysosomal biogenesis. *Science.* 2011;332:1429–33.
- Settembre C, Fraldi A, Medina DL, Ballabio A. Signals from the lysosome: a control centre for cellular clearance and energy metabolism. *Nat Rev Mol cell Biol.* 2013;14:283–96.
- Puertollano R, Ferguson SM, Brugarolas J, Ballabio A. The complex relationship between TFEB transcription factor phosphorylation and subcellular localization. *EMBO J.* 2018;37:e98804.
- Adams DR, Ron D, Kiely PA. RACK1, a multifaceted scaffolding protein: structure and function. *Cell Commun Signal.* 2011;9:22.
- Liao TJ, Jang H, Fushman D, Nussinov R. SOS1 interacts with Grb2 through regions that induce closed nSH3 conformations. *J Chem Phys.* 2020;153:045106.
- Chen M, Sawamura T. Essential role of cytoplasmic sequences for cell-surface sorting of the lectin-like oxidized LDL receptor-1 (LOX-1). *J Mol Cell Cardiol.* 2005;39:553–61.
- Deigner HP, Claus R. Stimulation of mitogen activated protein kinase by LDL and oxLDL in human U-937 macrophage-like cells. *FEBS Lett.* 1996;385:149–53.
- Grice GL, Nathan JA. The recognition of ubiquitinated proteins by the proteasome. *Cell Mol life Sci.* 2016;73:3497–506.
- Hu C, Dandapat A, Mehta JL. Angiotensin II induces capillary formation from endothelial cells via the LOX-1 dependent redox-sensitive pathway. *Hypertension.* 2007;50:952–7.
- Murdocca M, De Masi C, Pucci S, Mango R, Novelli G, Di Natale C, et al. LOX-1 and cancer: an indissoluble liaison. *Cancer Gene Ther.* 2021. Pubmed PMID:33402733.
- Li T, Fan J, Wang B, Traugh N, Chen Q, Liu JS, et al. TIMER: a web server for comprehensive analysis of tumor-infiltrating immune cells. *Cancer Res.* 2017;77:e108–e110.
- Hirsch HA, Iliopoulos D, Joshi A, Zhang Y, Jaeger SA, Bulyk M, et al. A transcriptional signature and common gene networks link cancer with lipid metabolism and diverse human diseases. *Cancer cell.* 2010;17:348–61.
- Wang B, Zhao H, Zhao L, Zhang Y, Wan Q, Shen Y, et al. Up-regulation of OLR1 expression by TBC1D3 through activation of TNFalpha/NF-kappaB pathway promotes the migration of human breast cancer cells. *Cancer Lett.* 2017;408:60–70.
- Lagergren J, Smyth E, Cunningham D, Lagergren P. Oesophageal cancer. *Lancet.* 2017;390:2383–96.
- Smyth EC, Lagergren J, Fitzgerald RC, Lordick F, Shah MA, Lagergren P, et al. Oesophageal cancer. *Nat Rev Dis Prim.* 2017;3:17048.
- Hong TS, Wo JY, Kwak EL. Targeted therapies with chemoradiation in esophageal cancer: development and future directions. *Semin Radiat Oncol.* 2013;23:31–37.
- Levy JMM, Towers CG, Thorburn A. Targeting autophagy in cancer. *Nat Rev Cancer.* 2017;17:528–42.
- Nassour J, Radford R, Correia A, Fusté JM, Schoell B, Jauch A, et al. Autophagic cell death restricts chromosomal instability during replicative crisis. *Nature.* 2019;565:659–63.
- Shay JW, Wright WE. Role of telomeres and telomerase in cancer. *Semin Cancer Biol.* 2011;21:349–53.
- Cumashi A, Ushakova NA, Preobrazhenskaya ME, D'Incecco A, Piccoli A, Totani L, et al. A comparative study of the anti-inflammatory, anticoagulant, anti-angiogenic, and antiadhesive activities of nine different fucoidans from brown seaweeds. *Glycobiology.* 2007;17:541–52.

35. Jiao G, Yu G, Zhang J, Ewart HS. Chemical structures and bioactivities of sulfated polysaccharides from marine algae. *Mar drugs*. 2011;9:196–223.
36. Vohra RS, Walker JH, Howell GJ, Homer-Vanniasinkam S, Ponnambalam S. The LOX-1 scavenger receptor cytoplasmic domain contains a transplantable endocytic motif. *Biochem Biophys Res Commun*. 2009;383:269–74.
37. Rabinowitz JD, White E. Autophagy and metabolism. *Science*. 2010;330:1344–8.
38. Liu P, Wang Y, Li X. Targeting the untargetable KRAS in cancer therapy. *Acta Pharm Sin B*. 2019;9:871–9.
39. Pylayeva-Gupta Y, Grabocka E, Bar-Sagi D. RAS oncogenes: weaving a tumorigenic web. *Nat Rev Cancer*. 2011;11:761–74.

ACKNOWLEDGEMENTS

We thank Dr. Jianping Zhang for small-animal PET imaging and Dr. Hengyu Jiang for SPR analysis. We thank Dr. Shuhui Sun for flow cytometric analysis and Dr. Yalin Huang and Jin Li for their excellent technical assistance in confocal microscopy.

AUTHOR CONTRIBUTIONS

C.L. and L.W. conceived the idea and designed the study. C.L., X.Y., and B.G. performed the experiments. G.L., G.H., and C.L. analyzed the data and wrote the manuscript. L.X., H.W., H.L., and S.L. provided assistance for experiments. C.Y., F.L., and J.Y. conducted human sample analysis. L.W. and Y.R. revised the manuscript. L.W., F.L., and J.G. obtained funding for the study and supervised it.

FUNDING

This work was supported by grants from the National Key Research and Development Program of China (2018YFC0910303) and the National Natural Science Fund (31870800, 32071272, and 82172803). The project was also supported by the Shandong Provincial Key Laboratory of Glycoscience & Glycotechnology (Ocean University of China).

COMPETING INTERESTS

The authors declare no competing interests.

ETHICS APPROVAL

The Ethics Committee of Basic Medical College of Fudan University.

ADDITIONAL INFORMATION

Supplementary information The online version contains supplementary material available at <https://doi.org/10.1038/s41418-021-00884-y>.

Correspondence and requests for materials should be addressed to Lan Wang.

Reprints and permission information is available at <http://www.nature.com/reprints>

Publisher's note Springer Nature remains neutral with regard to jurisdictional claims in published maps and institutional affiliations.